Visualization of active subretinal implants with external connections by high-resolution computed tomography

Florian Gekeler, Andreas Kopp, Helmut Sachs, Dorothea Besch, Udo Greppmaier, Eberhart Zrenner, Karl Ulrich Bartz-Schmidt, Peter Szurman

Visualization of active subretinal implants with external connections by high-resolution computed tomography

Florian Gekeler, MD [1*]
Andreas Kopp, MD [2]
Helmut Sachs, MD [3]
Dorothea Besch, MD [1]
Udo Greppmaier [4]
Eberhart Zrenner, MD [1]
Karl Ulrich Bartz-Schmidt, MD [1]
Peter Szurman, MD [1]

[1] Centre for Ophthalmology, University of Tübingen, Tübingen, Germany
[2] Department of Radiology, University of Tübingen, Tübingen, Germany
[3] Klinikum Friedrichstadt, Dresden, Germany
[4] Retina Implant AG, Reutlingen, Germany

[*] Corresponding author
Schleichstrasse 12-16
Germany
Tel.: +49-7071-2984761
Fax.: +49-7071-295215
E-mail: *gekeler@uni-tuebingen.de*

Word count (manuscript): 1182, with 6 images and 9 references

Keywords: retinal implant, prosthesis, computed tomography, subretinal

Statements

The Corresponding Author has the right to grant on behalf of all authors and does grant on behalf of all authors, an exclusive licence (or non exclusive for government employees) on a worldwide basis to the BMJ Publishing Group Ltd to permit this article (if accepted) to be published in BJO and any other BMJPGL products and sublicences such use and exploit all subsidiary rights, as set out in our licence (http://group.bmj.com/products/journals/instructionsfor-authors/licence-forms).

According to the journal's guidelines, the authors declare the following competing interests: (1) the retinal implant was manufactured and delivered by Retina Implant AG (RIAG), Gerhard-Kindler-Straße 8, D-72770 Reutlingen, Germany; (2) RIAG covered the direct costs of the study; (3) HS, EZ and FG are shareholders of RIAG; none of them receives payment or is employed by RIAG.

Summary

Two patients carrying an active subretinal implant with extra-ocular parts were examined by high-resolution computed tomography. Cranial scans were acquired in primary position and in 8 additional directions of gaze with eyes open and closed to demonstrate the mobility of the eyeball and the implant within the orbital cavity. 3 D images were constructed to visualize the path of the implant from the retro-auricular around the lateral orbital rim through the orbit and within the subretinal space up to the device's final para-foveal position. – Images were obtainable in high quality resulting in 3 D models illustrating all parts of the implant including the micro-photodiode array at the tip in the subretinal space. The implant followed eye movements in all directions of gaze, eye movements were only minimally restricted as described in previous publications. – Since all, except intra-ocular, parts of the implant evade direct examination computed tomography can help to assess technical integrity and the biocompatibility and biostability of retinal implants.

Introduction

Subretinal implants intend to restore visual function in diseases such as retinitis pigmentosa (RP) by replacing degenerated photoreceptors with microphotodiode arrays (MPDAs) [1-3]. Since it has been shown that more energy is necessary than is available through microphotodiodes [4] active subretinal implants with external connections have been constructed [5 6]. In this first clinical trial, a trans-cutaneous access in the retro-auricular space provided important advantages: it allowed direct evaluation of electrode parameters such as impedance and charge transfer; and second, it provided maximum security and stability for stimulation and driving circuits of the subretinal device. Future implants, however, will be fully implantable with wireless transmission of signals and energy.

After implantation, ophthalmologic examination is limited to external aspects and to the ocular fundus where the implant can be directly seen up to the point of trans-choroidal passage. However, the subdermal cable, the connection of the cable to the polyimide foil in the temporal fossa, and the passage of the foil around the lateral orbital rim through the orbit to the trans-choroidal passage, all of these evade direct examination. Some groups applying epiretinal prostheses use similar extra-ocular routes, [7 8] while other groups prefer an all-intraocular approach [9].

In order to visualize an implant with extra-ocular parts *in vivo*, to evaluate it under strong eye movements, and to examine the tissue surrounding it, we have performed this exploratory study using high-resolution computed tomography (CT).

Patients, Material and Methods

Two patients were included, both were male and suffered from end-stage RP with light perception. They gave written informed consent; all procedures adhered to the Declaration of Helsinki.

Patient 1 (P1; 44 years old) was implanted in October 2005 in his right eye. Although the study period and insurance covering was granted for 4 weeks by the local ethics committee the patient refused explantation; he still carries the implant. The device's extra-corporeal parts in the retro-auricular area were removed and the skin closed after 12 months.

P2 (42 years old) was implanted in October 2007. Because of beginning implant failure the extra-ocular parts were removed three months later (the study period was granted for 4 months at this point) and the intra-ocular parts 10 months post-operatively on the patient's decision.

The implant consisted of 4 connected parts (details are given in fig.1*)*. The subretinally placed tip comprised two different entities: a MPDA with 1,500 microphotodiodes for light-driven stimulation and a 4*4 electrode array for direct electrical stimulation.

A SOMATOM Definition® (Siemens AG, Forchheim, Germany) CT scanner was used, collimation was 0.5 mm at 120 kV and 100 mA.

DICOM (Digital Imaging and Communications in Medicine) images of P1 were segmented using Amira® (Visage Imaging GmbH, Berlin, Germany), exported as VRML (virtual reality modeling language)-data and rendered in Maxon Cinema 4D® (Maxon Computer GmbH, Friedrichsdorf, Germany). Images of P2 were segmented and rendered by the CT scanner's Leonardo® workstation software (Siemens AG, Erlangen, Germany) to generate 3 D images. Final images and colors were obtained using Photoshop® (Adobe Systems Incorporated, San Jose, CA, USA).

Scans were taken in primary position (patient looking straight) with eyes open and eyes closed, and in 8 cardinal directions of gaze: up, down, left, right, upper right, upper left, lower right, lower left.

Results

CT scans were obtainable in high quality with only minor adjustments to regular examination parameters for thin slice orbital exams. Virtually all parts of the implant were clearly visible: the subretinal part with the 4*4 array and the thicker portion resembling the MPDA, the golden connection lanes on the polyimide foil in the subretinal space following the curvature of the posterior eyeball, its bend at the choroidal/scleral passage, the fixation pads for episcleral suturing, the foil's path through the orbital cavity and around the lateral orbital rim, the connection pad to the silicone cable in the temporal fossa, the silicone cables way to the retro-auricular space, and the metal fixation clamp on the skull.

Fig. 2 shows 4 transversal sections of P1 with moderate soft tissue reaction to the orbital parts of the implant near the lateral orbital rim; all other structures within the orbital cavity, including sclera, optic nerve and eye muscles seem unaffected.

Fig. 3 shows the steps to segment an original 2 D image to obtain a 3 D image as shown in figs. 4-6.

Fig. 4 shows 3D-reconstructions of P1 from different angles along a transversal plane around the implant. In 3D reconstructions relative dimensions of various implant parts were evaluated to assess if such measurements would yield meaningful results. The MPDA measured exactly 3 mm * 3 mm and was taken as reference in its largest presentation in CT images. The silicone cable measured 3.19 mm (3 mm in reality; always averages of various measurements), the connection pad 9.6 mm (12 mm in reality; however, this structure was curved in the patient which was not measurable), the wider polyimide foil at the orbital rim 2.7 mm (2.5 mm in reality), the subretinal polyimide foil 1.5 mm (1.5 mm in reality).

Fig. 5 shows similar reconstructions of P2 who still carried the entire implant showing also the metal clamp and the extra-corporeal part.

Fig. 6 shows 4 views of P1 at three different directions of gaze: straight, and upper right and lower left causing maximum deflections in the orbit. Eye movements were minimally restricted in photographic gaze analysis, but were not described as disturbing [5].

Under ftp://134.2.124.64/home (login and password: ‘BJO’) a self-maneuverable 3D-animation can be downloaded and viewed using Quicktime® (Apple Inc., Cupertino, CA, USA).

Discussion

CT has proven feasible in two patients with subretinal implants yielding strikingly illustrative pictures. CT is cost-effective and can provide higher detail than any other technique including ultrasound sonography, which also demonstrates bad penetration depth in bone, and magnetic resonance imaging, which is not recommendable for such kind of implants with cable wiring due to possible danger to implants and surrounding tissue through high-frequency electro-magnetic fields. While radiation exposure of CT scans, especially if performed frequently for study purposes, must be mentioned, CT constitutes the only means to visualize the implant's parts outside of the eye in high resolution which in our case can be estimated to be around 0.1 mm. CT images are readily transferrable to construct a 3D image in external software. In these, meaningful measurements of dimensions of the implant could be performed.

CT pictures of such high resolution can show all technical aspects of the implant and give valuable indications for research purposes and in case of technical problems. Images also deliver data on the tissue reaction (biocompatibility) and can visualize the behaviour of the implant under eye movements. And, last but not least, such three dimensional images and animations are excellent for illustrations and instructional purposes.

Epiretinal as well as subretinal implants currently mostly utilize extra-ocular connections for energy and signal conduction. Since they are still implanted under clinical trial conditions adequate monitoring tools are mandatory to study the integrity of the device (biostability) and the body's reaction to it (biocompatibility). We believe that high-resolution CT scans can contribute to the success of these implants by delivering adequate imaging material.

Legends

Figure 1

Photographs of (a) the subretinal implant and (b) the fixation clamp.

(a) The subretinal implant consists of: 1.) a subretinal part (polyimide foil; 20 µm thick, 1.5-2.5 mm wide, ca. 22 mm long) with 2 entities at its tip: a 4*4 electrode array and a microphotodiode array with 1.500 photodiodes lying para-foveally. 2.) an orbital part of the polyimide foil with fixation pads after choroidal and scleral perforation; at ca. 62 mm from the implant's tip a silicone pad is attached to the polyimide foil for suture fixation to the lateral orbital rim which connects via a connection pad to 3.) a subdermal silicone cable (diameter 3 mm) containing 22 spiralled gold flexes; after clamp fixation it perforates the retro-auricular skin. 4.) an extra-corporeal part of the silicone cable with a plug to an external generator for control signals and energy delivery.

(b) A clamp was built from surgical steel for fixation of the implant on the scull bone in the retro-auricular region. The clamp consisted of a base plate which was screwed into the scull bone and a cover plate with a recess to jam the silicone cable onto the base plate (scale is in mm).

Figure 2

Original transversal CT images of P1.
a. In this section the foil with gold connection lanes around the lateral orbital rim, within the orbit and its course on the eyeball with the scleral fixation can be seen. In the region at the lateral orbital rim there is moderate soft tissue proliferation surrounding the implant in comparison to the contra-lateral side. All other orbital structures in this and sections b-d of this figure, including sclera, optic nerve, and eye muscles are normal.
b. In this section the course of the polyimide foil with the gold connection lanes can be followed from the orbital rim; on the posterior pole the implant's tip in the subretinal space is visible.
c. This section shows the full extent of the subretinally implanted microphotodiode-array with a size of approximately 3 mm.

d. In this section the connection pad in the temporal fossa produces the typical radiating artifacts from metal.

Figure 3

Steps for segmentation of original images to obtain 3D reconstructions.
a. This screenshot shows one original image on the left side which was chosen from the sections on the right side.
b. This screenshot shows the segmentation tool of the software; the segmented parts consisting of bone and implant are shown in red.
c. This screenshot shows one raw version of a 3 D reconstruction from segmented images.

Figure 4

3 D reconstructions of CT scans of patient 1.

The scans were taken 21 months after implantation; the external parts of the implant and the metal clamp had been removed 12 months after implantation when granulation tissue had occurred at the skin perforation site and the implant was not used any more due to regulation by the ethics committee. – All parts of the implant are clearly visible: 1. the subretinal tip with an MPDA and the direct stimulation electrodes (coloured blue; colors do not represent differences in Hounsfield units, but rather were applied later to a 3D raw image serve better visualization), 2. the fixation pads for episcleral fixation of the polyimide foil (red), 3. the orbital part of the polyimide foil, 4. the connection of the foil to the silicone cable in the temporal fossa, 5. the silicone cable leading subperiostally to the retro-auricular space (green).

Figure 5

3 D reconstructions of CT scans of patient 2 with a subretinal implant.

The scans were taken 2 months after implantation; the implant was complete with the clamp in the retro-auricular space and its external parts. – All parts of the implant are also clearly visible as in fig. 1 and have been coloured identically; in addition, the metal clamp is coloured turquoise.

Figure 6

Orbital details of CT scans in 3 D reconstructions under different directions of gaze.

Of the 9 directions of gaze scanned only those where implant movements are extreme are shown, i.e. in direction or away from the direction of the orbital entry point. The implant's movements can be detected by comparing the position of the blue subretinal tip and the episcleral fixation pads of the polyimide foil (red).

Quicktime® animation (downloadable)

Similar images as in fig. 1 were used to compose this self-maneuverable animation which additionally allows cranial, caudal, and oblique views. Please go to ftp://134.2.124.64/home (login and password: 'BJO'; Quicktime® is obligatory to maneuver the images).

References

1. Chow AY, Peachey NS. The subretinal microphotodiode array retinal prosthesis [letter; comment] *Ophthalmic Research* 1998;30(3):195-98.
2. Zrenner E. Will retinal implants restore vision? *Science* 2002;295(5557):1022-25.
3. Zrenner E, Stett A, Weiss S, Aramant RB, Guenther E, Kohler K, et al. Can subretinal microphotodiodes successfully replace degenerated photoreceptors? *Vision Research* 1999;39(15):2555-67.
4. Stett A, Kohler K, Weiss S, Haemmerle H, Zrenner E. Electrical stimulation of degenerated retina of RCS rats by distally applied spatial voltage patterns. *Invest Ophthalmol Vis Sci* 1998;39:902S.
5. Besch D, Sachs H, Szurman P, Gulicher D, Wilke R, Reinert S, et al. Extraocular surgery for implantation of an active subretinal visual prosthesis with external connections: feasibility and outcome in seven patients. *Br J Ophthalmol* 2008;92(10):1361-8.
6. Gekeler F, Sachs H, Szurman P, Guelicher D, Wilke R, Reinert S, et al. Surgical Procedure for Subretinal Implants With External Connections: The Extra-Ocular Surgery in Eight Patients. *Invest Ophthalmol Vis Sci* 2008 49: E-Abstract 4049.
7. Greenwald SH, Horsager A, Humayun MS, Greenberg RJ, McMahon MJ, Fine I. Brightness as a function of current amplitude in human retinal electrical stimulation. *Invest Ophthalmol Vis Sci* 2009;50(11):5017-25..
8. Hornig R, Laube T, Walter P, Velikay-Parel M, Bornfeld N, Feucht M, et al. A method and technical equipment for an acute human trial to evaluate retinal implant technology. *J Neural Eng* 2005;2(1):S129-S34.
9. Roessler G, Laube T, Brockmann C, Kirschkamp T, Mazinani B, Goertz M, et al. Implantation and explantation of a wireless epiretinal retina implant device: observations during the EPIRET3 prospective clinical trial. *Invest Ophthalmol Vis Sci* 2009;50(6):3003-8.

a

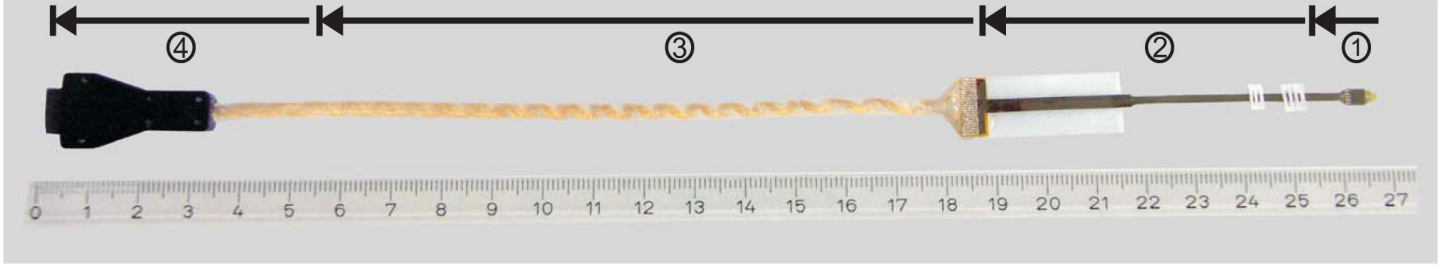
④
③
②
①
0 1 2 3 4 5 6 7 8 9 10 11 12 13 14 15 16 17 18 19 20 21 22 23 24 25 26 27

b

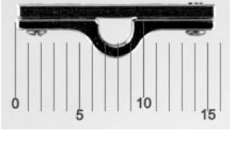
0
5
10
15

a

b

c

d

a

b

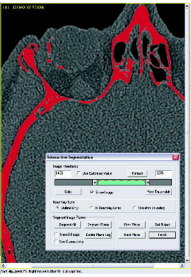

c

a

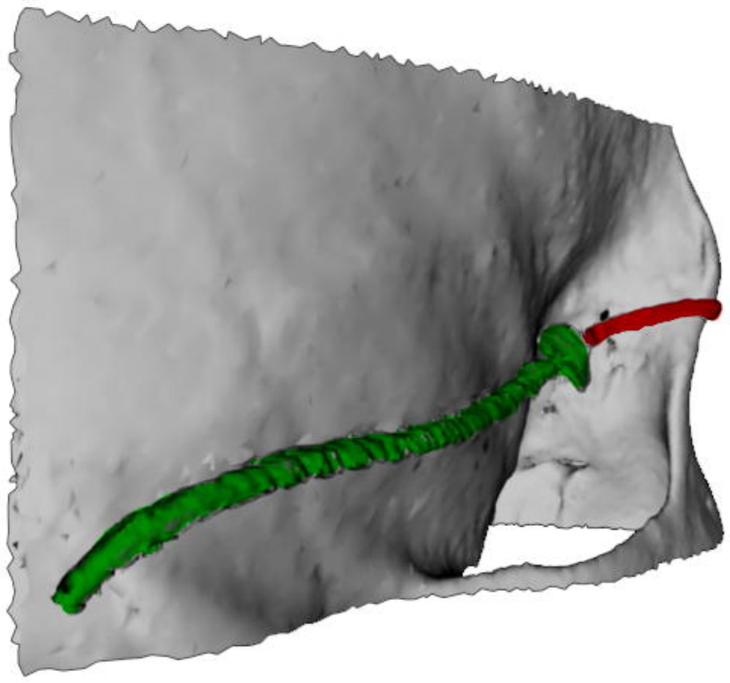

b

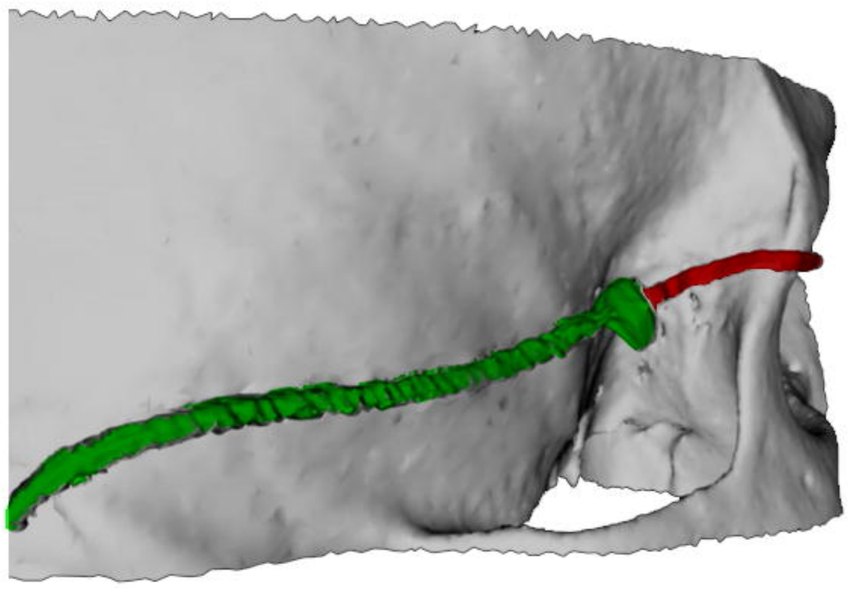

c

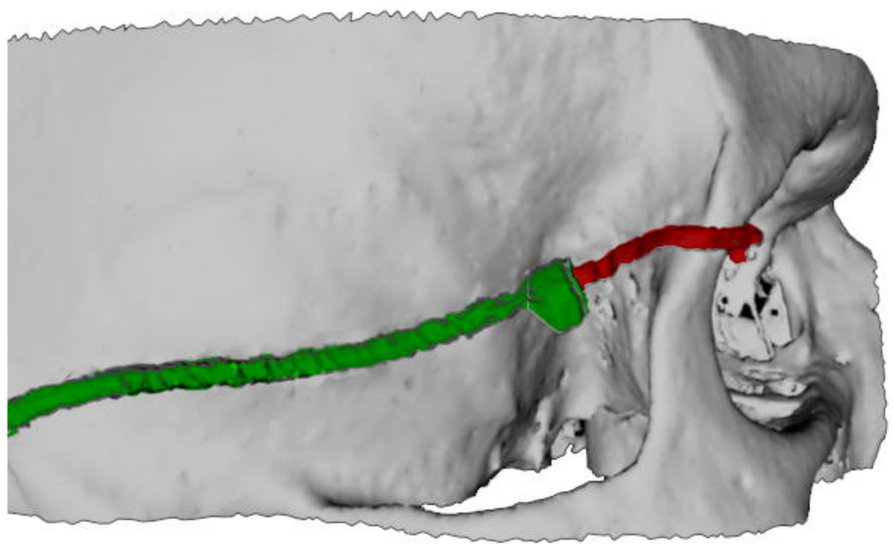

d

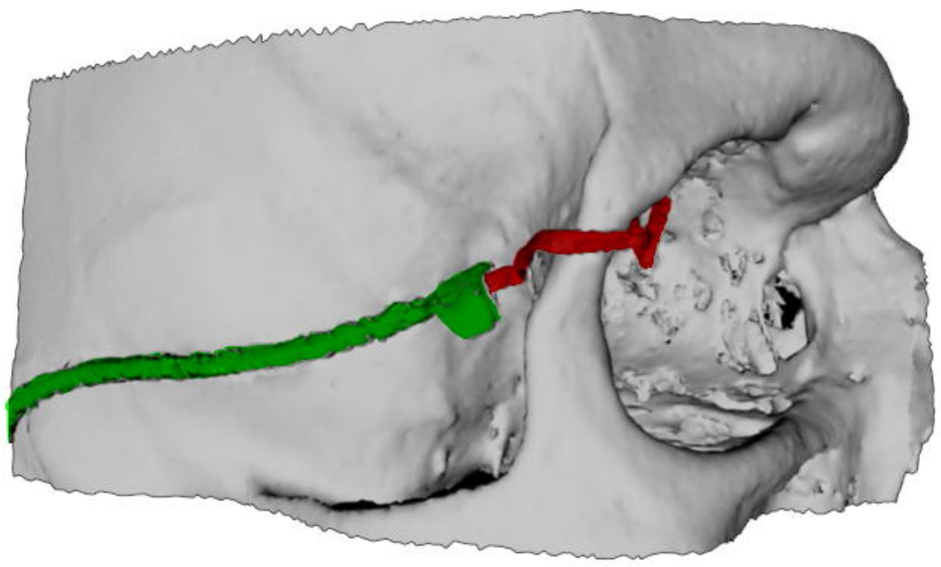

e

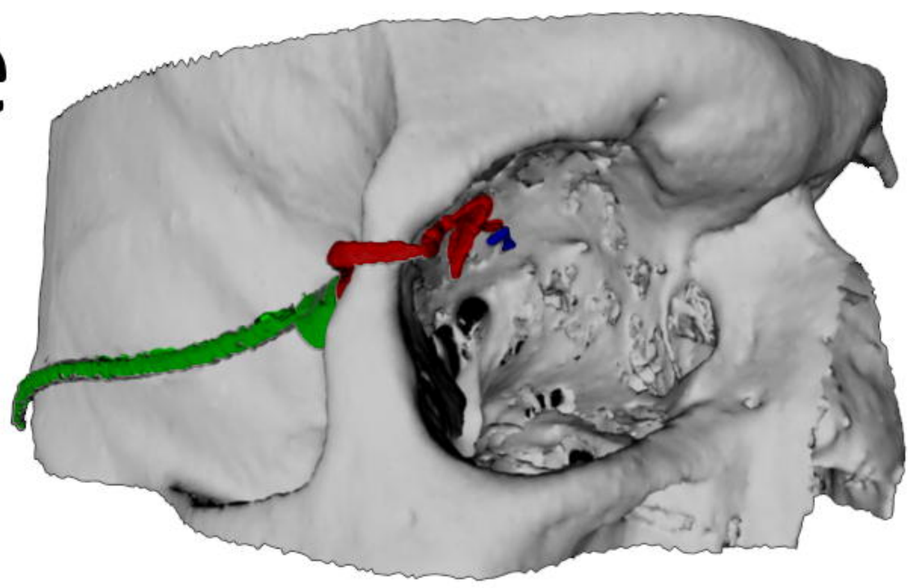

f

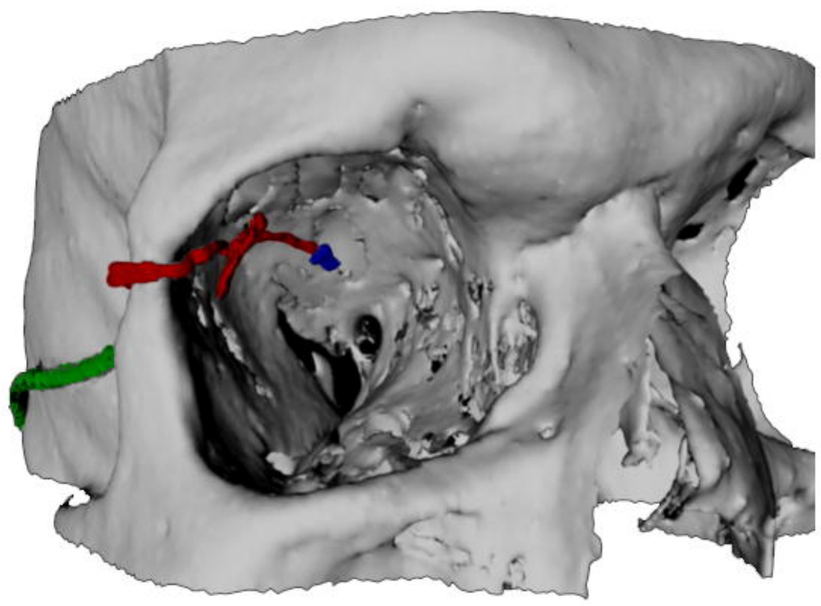

g

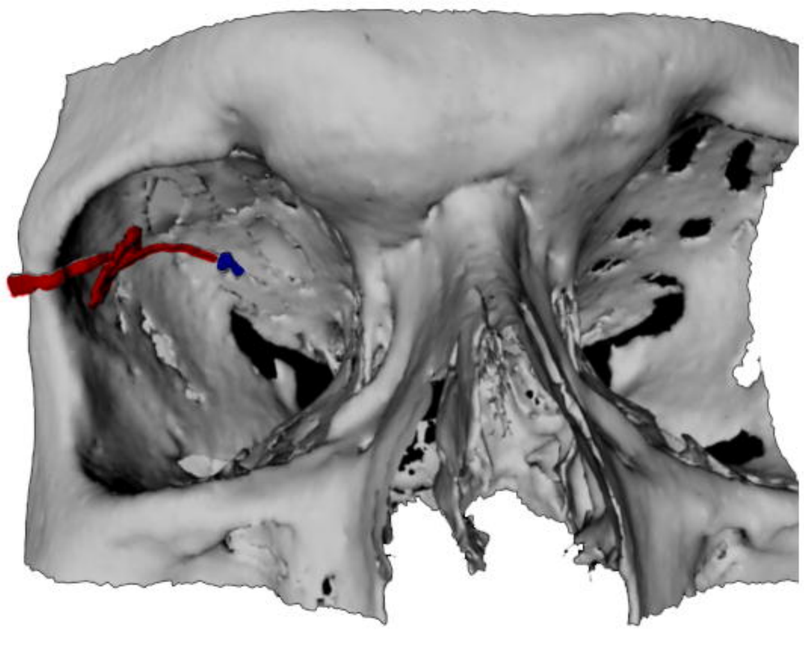

h

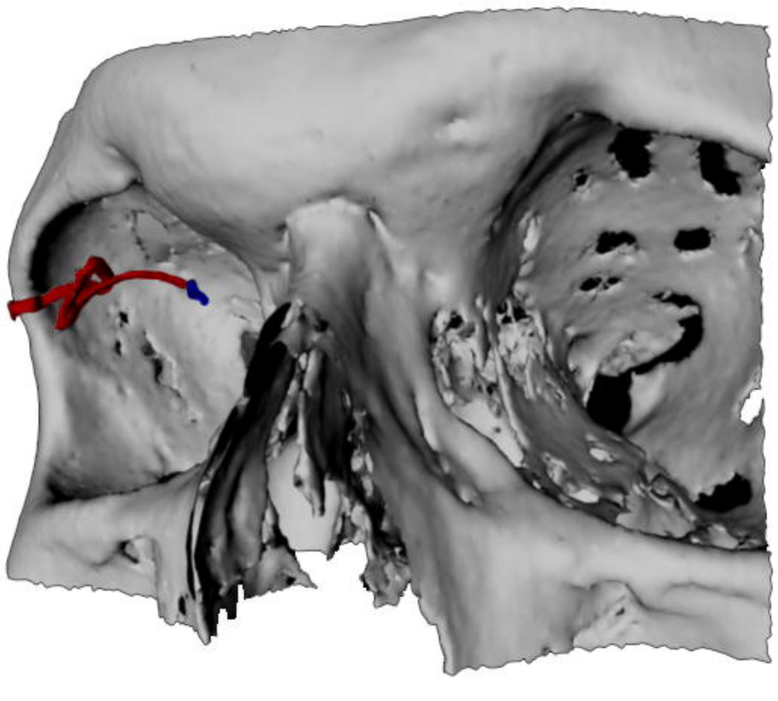

a

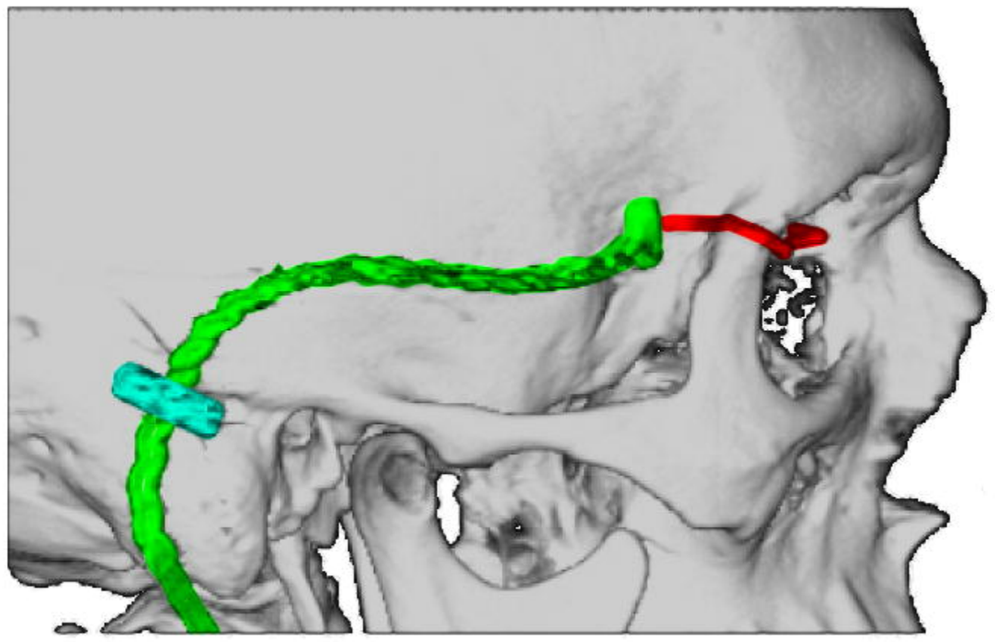

b

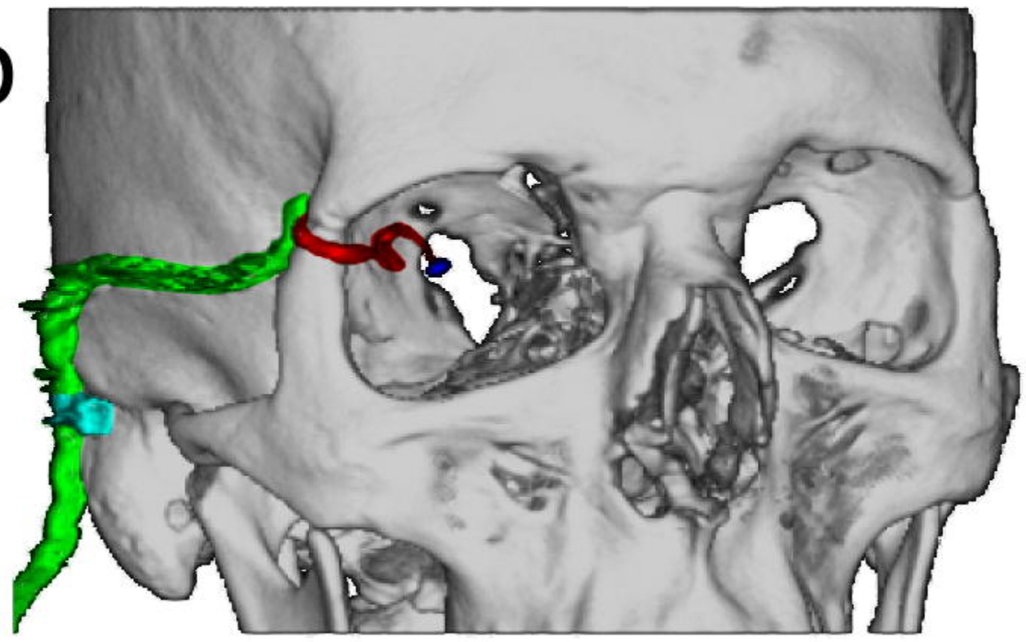

c

d

angle of observation

lateral | 45° | frontal | 120°

direction of gaze

right, up

straight

left, down